Biocybernetics and Biomedical Engineering 44 (2024) 609–616

Contents lists available at ScienceDirect

Biocybernetics and Biomedical Engineering

journal homepage: www.elsevier.com/locate/bbe

Static compression optical coherence elastography for the measurement of porcine corneal mechanical properties ex-vivo

Zachery Quince [a,b,*], David Alonso-Caneiro [b,c], Scott A. Read [b], Damien G. Harkin [d], Michael J. Collins [b]

[a] School of Engineering, University of Southern Queensland, Springfield, Queensland, Australia
[b] Contact Lens and Visual Optics Laboratory, Centre for Vision and Eye Research, Optometry and Vision Science, Queensland University of Technology, Brisbane, Australia
[c] School of Science, Technology and Engineering, University of Sunshine Coast, Petrie, Queensland, Australia
[d] Centre for Vision and Eye Research, School of Biomedical Sciences, Faculty of Health, Queensland University of Technology (QUT), Brisbane, QLD, Australia

ARTICLE INFO

Keywords:
Optical coherence elastography
Boundary segmentation
Animal model

ABSTRACT

Significance: The biomechanical properties of the cornea are important for vision and ocular health. Optical coherence elastography (OCE) has the potential to improve our capacity to measure these properties.
Aim: This study tested a static compression OCE method utilising a commercially available optical coherence tomography (OCT) device, to estimate the Young's modulus of *ex-vivo* porcine corneal tissue.
Approach: OCT was used to image corneal tissue samples before and during loading by static compression. The compressive force was measured with a piezoresistive force sensor, and tissue deformation was quantified through automated image analysis. Ten *ex-vivo* porcine corneas were assessed and the corneal thickness was also measured to assess the impact of corneal swelling.
Results: An average (standard deviation) Young's modulus of 0.271 (+/- 0.091) MPa was determined across the 10 corneas assessed. There was a mean decrease of 1.78 % in corneal thickness at the end of the compression series. These results showed that there was a moderate association between corneal thickness and the Young's modulus recording ($R^2 = 0.274$).
Conclusions: Optical coherence elastography utilising clinical instrumentation, can reliably characterise the mechanical properties of the cornea. These results support the further investigation of the technique for *in-vivo* measurement of the mechanical properties of the human cornea.

1. Introduction

The field of ocular biomechanics is undergoing rapid and continuous development, especially with advances in medical imaging technologies that are able to describe the biomechanical properties of a range of ocular tissues [1–4]. Despite the advancements in the field, the mechanical properties of the cornea are still not fully understood or easily characterized for several reasons including: the complex nature of this layered structure, the number of factors that can affect the measurement (i.e. intraocular pressure and tissue thickness), and the added challenge associated with imaging transparent tissue [2,5]. Corneal diseases, such as keratoconus, which have a significant impact on vision and quality of life, are strongly linked to changes in the mechanical properties of the corneal tissue [2,5]. Therefore, the development of methods to characterize tissue mechanical properties are important for the ophthalmic field.

Fluid filled tissues exhibit two sets of mechanical properties: elastic and viscous, which is typically known as viscoelastic behaviour. These properties determine how the tissue responds to a particular load or deformation. The Young's modulus, which is a fundamental measurement to characterize the mechanical properties of a material, measures the ratio of stress to strain, or in other words, how much the material has deformed under an applied load. This metric assumes a linear relationship between stress and strain. However, for biological materials, a linear or non-linear viscoelastic response may be observed, so care should be exercised [6,7]. For a static load, like the one applied in static compression optical coherence elastography (OCE), the impact of the non-linear response will be diminished due to the low strain rates and

* Corresponding author.
E-mail address: zach.quince@unisq.edu.au (Z. Quince).

https://doi.org/10.1016/j.bbe.2024.08.006
Received 1 May 2024; Received in revised form 2 July 2024; Accepted 17 August 2024
Available online 28 August 2024

previous reporting of linearity in corneas. A study by Kling et al. [8] demonstrated that the stress/strain relationship of human corneas was linear for a low level of stress (4 kPa) using a quasi-static loading method. Interestingly, porcine corneal tissue has been shown to have a more linear response to loading than that of human corneal tissue [5,6].

To date, a number of studies have been proposed on the application of OCE for measurement of ocular biomechanics. In order to stimulate the tissue, non-contact methods such as air-puff have been applied to deform the tissue and measure the mechanical properties (response) of the cornea. This involves tracking the movement caused by the air-puff between sequential images and relating these tissue changes or wave propagation to the mechanical properties of the underlying tissue [9–11]. Wang and Larin [12] investigated the use of air-puff OCT to generate shear waves in tissue mimicking agar phantoms and ex-vivo rabbit corneas. Dorronsoro et al. [13] used an air stream to deform the cornea and imaged the displacement through a spectral OCT. Other non-contact methods that have been used include an ultrasound air coupled approach that generates a displacement through excitation waves [14], an acoustic approach to generate displacement [15], and an ambient pressure modulation to create a displacement that can be imaged via OCT [16]. Similar to early applanation tonometry methods, several contact OCE methods have also been applied to the eye. Ford et al. [17] employed a gonioscopy lens to mechanically load a fixed, pressurised *ex-vivo* globe whilst being imaged by a custom Fourier domain optical coherence tomography (OCT) instrument. Ramier et al. [18] used a contact based piezoelectric transducer to propagate surface acoustic waves in ex-vivo porcine corneas. The movement was tracked by a custom-built OCT system and the displacement was analysed by separating the frequencies of the waves using a Fourier transform. Ramier et al. [19] further investigated this application to in-vivo human corneas to measure the shear modulus. De Stefano et al. [20] used a static compression method to investigate depth dependant characteristics of the cornea in patients with and without keratoconus, using a custom-built OCT instrument. The instrument had a lens attached to a translation stage with an in-built force sensor to track the applanation force. Using this setup, the relationship between displacement and load were measured, showing that there was more deformation with the same load in keratoconus patients compared to normal corneas. This study is one of the first to apply contact OCE methods with *in-vivo* corneal tissue.

While a number of studies in the field to date have demonstrated the potential of OCE methodologies to extract the mechanical properties of materials [21,22] and corneal tissue [8,18,20,23], it is worth noting that although most studies explore the stress/strain relation of tissue, the majority of previous studies have not characterised the Young's modulus metric. In some instances, this is because the technique may not be compatible with this metric, while in others, the authors have not considered this approach. It should be noted that several of the previous studies cited used custom-built OCT devices which may be challenging to implement into a clinical setting due to the need for non-commercial instruments. The application of OCE imaging to corneal tissue is in its infancy and further development is needed to enable the application of this technique in a clinical setting in the future. This study aimed to develop a static compression OCE method utilising a commercially available OCT device, to estimate the Young's modulus of *ex-vivo* corneal tissue. To ensure that the method was suitable for a full and rapid clinical translation, the method was required to be undertaken with little to no modifications or custom-built equipment and the analysis method to be rudimentary to be achieved via hand calculations.

2. Materials and methods

2.1. Theoretical principles

The study builds upon the OCE experimental setup presented in [21], which was designed to test mechanical properties of contact lens materials. In the current study, the methodology is adapted to assess ex-vivo corneal tissue, which was uniaxially compressed via a glass plate and imaged before and during loading, generating a tissue deformation that is assumed to be uniaxial in nature. It should be noted that the first image of the sequence (the "before loading") was captured with a small pre-load of approximately 1 % strain, determined by using an electronic force sensor. This pre-load is required to remove any surface anomalies that could cause inaccuracies while analysing the data. A similar pre-load condition was applied in [22], demonstrating good performance to measure contact lens mechanical properties. Other studies have also used a pre-load approach in their imaging protocols [24,25].

The OCE method utilises a commercially available clinical spectral domain OCT (Heidelberg Spectralis, Heidelberg Engineering GmbH, Germany) to capture high resolution image of the tissue during pre-load and compression. The OCT uses a super luminescent diode (SLD) operating at a central wavelength of 870 nm and has an optical resolution of 7 μm (axial) and 30 μm (lateral). The axial range of the OCT is 1.9 mm (in tissue). A semi-automated, boundary segmentation method, is then used to track the change in thickness between the initial pre-loaded and the compressed images. To calculate the Young's modulus of the cornea, the stress and strain of the tissue needs to be determined. The Young's modulus (E, in MPa) of the material is derived as the ratio between the stress (σ, in MPa) and the strain (ε, unitless) values using (Eq. (1)) (assuming uniaxial compression).

$$E = \sigma/\varepsilon \tag{1}$$

In this study, the strain can be estimated by measuring the cornea boundaries before and during compression using the corresponding OCT images and the calculation given by (Eq. (2)):

$$\varepsilon = (L_o\text{-}L_n)/L_o \tag{2}$$

Where, Lo is the 'original' thickness of the contact lens before compression and Ln is the 'new' thickness of the contact lens during compression, both in μm. Finally, the stress value is estimated from the force (F) that the cornea is under during compression and the compression area (A) using (Eq. (3)):

$$\sigma = F/A \tag{3}$$

where, F is the force in Newtons (N) and A represents the cross-sectional area in m2 measured by imaging the surface of the corneal tissue using the en-face scanning laser ophthalmoscope (SLO) image (instrument's front on image) to extract the radius. See [21,22] for further information on the theoretical principles behind the technique.

There are several assumptions and limitations of the current method. The corneal tissue is assumed to be a homogeneous material [7,26]. Whilst the structure of the cornea is not uniform, with the current image analysis method, the stress that different layers experience during compression cannot be examined. As a result, the measurement extracted from this method represents a global metric of the entire tissue cross-section. Additionally, due to the properties of the cornea, it can exhibit non-linear behaviour and may not produce a linear stress/strain relationship [7,26]. Given the 'static' nature of the method, where the measurements cannot be captured instantaneously or continuously, this viscoelastic behaviour is assumed to be negligible for the current study. Thus, it is assumed that given the time gap between loading and the measurement, the cornea has reached an equilibrium state, in which any time-related variations of the loading had dissipated.

2.2. Instrumental setup

The instrumental setup consists of two sides, the imaging side, and the sample side. The setup is consistent with that reported in previous studies The corneal tissue was imaged using a volumetric scanning protocol (approximately 8.325 mm horizontal and 6.39 mm vertical). The protocol captured 21 individual B-scans orthogonal to the incident beam that contained 768 A-scans each, with each B-scan 277 μm apart

vertically and 8.325 mm scanned horizontally. The OCT images have an axial resolution of 3.87 μm and a transverse resolution of 10.8 μm. After the pre-load images were acquired, the corneas were compressed until the force sensor recorded a value that corresponded to a strain rate of between 7–13 %. This range was based on previous results with the method for a material that recorded a Young's modulus of 0.2 MPa with a 50 % water content. This approach was trialled during pilot studies and showed that it was a consistent force (0.2 N) to compress the lens to achieve a strain rate of 7–13 %. The variation in strain was due to the variance in the output voltage recorded by the force sensor and the supply voltage. All corneas were imaged using this force, both inter-trials and intra-trials. The assumption of linearity has been demonstrated in previous studies over this range of strain [4]. These calculations were informed by previous studies that found the Young's modulus was approximately 0.2 MPa for porcine corneal tissue [27]. Each of the corneas were imaged three times, using the above protocol. The corneas were compressed for a period of approximately 30 s for imaging during each of the three trials. For each cornea, the whole imaging process took about 5 min.

2.3. Image analysis

Once the images were captured, they were exported from the OCT for analysis. The first step in the analysis was a visual review of the data to ensure that the boundaries were visible, and the images were free of artifacts that would prevent their processing. After which, the posterior and anterior boundaries of the corneal tissue were extracted. A number of the pre-load images did not have a visible posterior boundary as the corneal thickness was close to the axial imaging depth of the OCT instrument. However, since the width of the B-scans was wider than the imaged tissue sample, the back surface of the sample mount was always visible on either side of the tissue, even if the posterior boundary of the tissue was not visible. This optical distortion in the OCT image arises from the refractive index of the corneal tissue [28]. It causes the portion of the sample mount separated from the compression plate by air (n = 1) to appear optically closer to the compression plate than the portion of the sample mount separated from the compression plate by corneal tissue (n = 1.376) (Fig. 1). Taking advantage of this optical distortion, it was possible to estimate where the posterior surface of the cornea is located, even if the posterior boundary was not visible. Thus, to estimate the posterior boundary of the cornea, manual segmentation of this boundary was undertaken using the artefacts caused by the air gap as shown in Fig. 1, and then adjusting for the corneal refractive index to determine the true boundary position. To visualize the effect of the optical distortion, Fig. 1 shows a B-scan with the posterior boundary corrected for the corneal refractive index and compares this to the manually segmented line using the back surface of the sample mount as a reference. The lengths of both lines are matched to the anterior surface, which was segmented using a semi-automatic approach. For each volumetric scan, all 21B-scans were segmented, including the anterior and posterior corneal boundaries and the manual selection of the lateral locations of the sample mount (points A and B in Fig. 1) and generating a line between these two points. The semi-automatic approach for the anterior boundary required the two lateral sides of the compression plate to be defined though a manual selection and used a graph-search method to segment the images based on the boundary reflectivity [21,22,29,30]. There were several B-scans per trial that were excluded from analyses, due to the cornea not being present in that region of the volume scan. These typically occurred for the top or bottom B-scans of the volume scan.

Once the segmentation was completed, there were several parameters and metrics that were extracted. The axial thickness of both the pre-load and compressed volumetric scans were calculated and plotted as corneal thickness maps, as seen in Fig. 2(a) & (b). The thickness of the cornea was extracted in both pre-loaded and compressive states. The strain was calculated, using the change in thickness between the pre-load and compression images. This strain was then plotted as a map as seen in Fig. 2(c). As the stress was determined from the force and the area, this was then applied to the strain and used to generate a Young's modulus map (Fig. 2(d)). The small variations in thickness maps and associated strain and Young's modulus maps that can be seen in Fig. 2 is due to the finite ability of the semi-automated analysis procedure to produce a segmentation line that will 'snap' to the top of each pixel. This small variation in the segmentation line, which typically are only a few pixels, cause a small difference in thickness, and subsequent metrics (strain and Young's modulus).

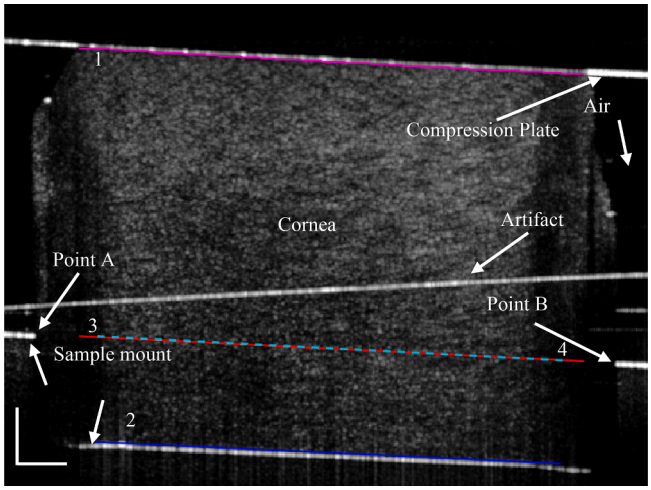

Fig. 1. Cross-sectional B-scan of the compressed cornea under OCT imaging showing the sample mount and compression plate (scale – 200 μm axial, 500 μm lateral). The pink line (1) represents the anterior surface of the cornea that was segmented using a semi-automatic boundary method. The blue line (2) represents the posterior surface of the cornea, which was segmented using a semi-automatic method. The cyan line (3) is the blue line corrected for the corneal refractive index (n = 1.376). The dashed red line (4) is the manually segmented posterior surface that is determined by fitting a line between the location of the sample mount on either side of the corneal tissue (point A & B) that are separated from the compression plate by air (n = 1). The red line has been shortened to the same length as the anterior surface. The location of the cyan line and red line match well. The artifact shown in this image is the 'mirror-image' of the compression plate, which occurs as part of the Fourier transform in OCT imaging.

To characterise the tissue, two metrics were extracted from the data: the Young's modulus and strain values which were calculated using Eq. (1) and Eq. (2) respectively. These were determined using the mean value of the strain and median value of the Young's modulus maps. To determine the mean for the strain and Young's modulus maps, each of the extracted data points from the comparisons between the pre-load thickness and the compression map were averaged across the entire map. These two descriptive statistics were chosen since they were found to be the most accurate and repeatable in a previous study using similar methods [21,31]. The method in [21] was modified, in which a Young's modulus point (location) was manually selected using the maximum thickness in the pre-load image as the point of comparison. In this study, an average across the region was chosen which also removes any bias in the selection process and aligns more closely with the assumption that the material is homogenous.

2.4. Materials

Due to the difficulty of accessing human donor tissue, *ex-vivo* porcine eyes were used in this study. Porcine corneas have a similar anatomy to human eyes, with a collagenous stroma making up the bulk of the tissue and a reported thickness of ~ 850 μm [32], and have been used in several previous corneal biomechanical studies [33–35]. Ten porcine

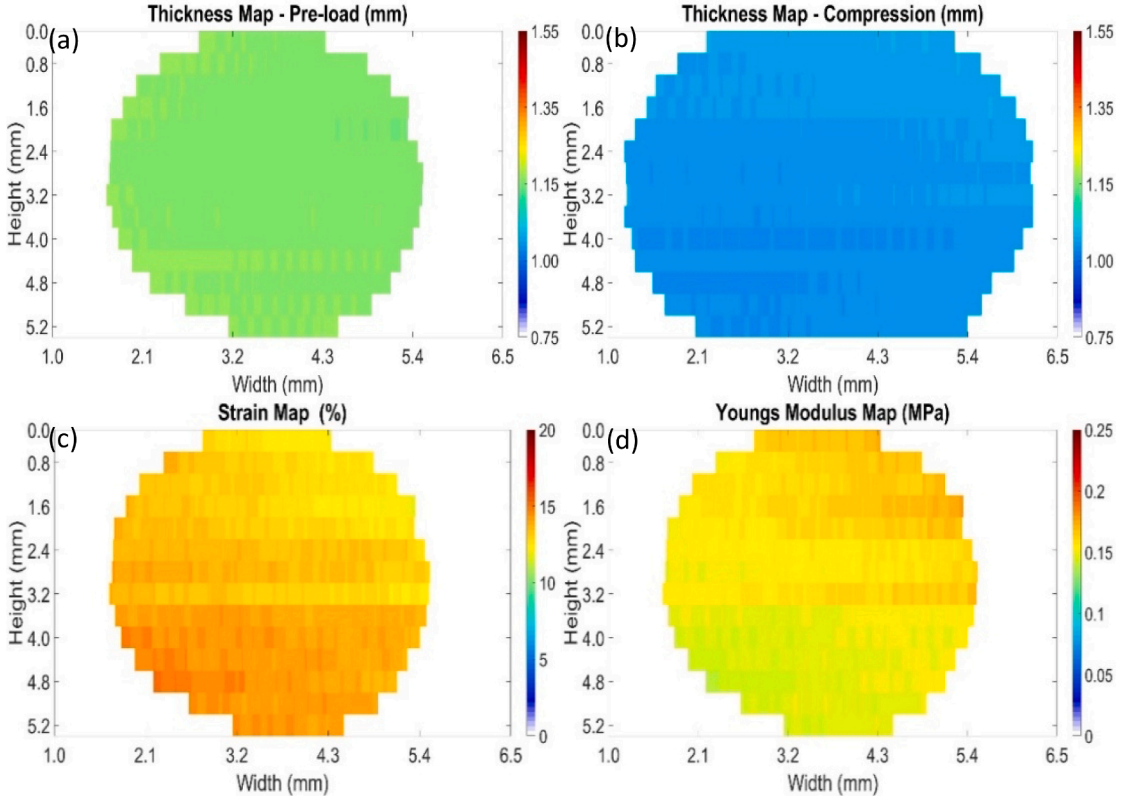

Fig. 2. Example of thickness, strain and Young's modulus maps for an ex-vivo porcine cornea recording showing the pre-load: (a) and compressed; (b) corneal thickness maps, the associated strain; (c) and the Young's modulus; (d) maps of the cornea. The width of the compression thickness map (a vs. b) changes as the force of the compression pushed the tissue sample resulting in a wider and thinner corneal sample.

globes (age ~ three months) were collected from a local abattoir, with enucleation happening immediately post-mortem. Due to the eyes being collected from an abattoir, a notification of the intended use of the tissue was approved by the QUT research ethics committee. Initially, the corneas were dissected from the globe using a scalpel and scissors. A small scleral ring was left attached to the tissue, in order to limit the amount of fluid that could be absorbed by the cornea. When the cornea was ready to be imaged, a central disc was extracted using a 6 mm biopsy punch (KAI Group, Tokyo, Japan). The globes were stored in a 7.4 pH phosphate buffered saline solution at approximately 5° Celsius. The corneas were dissected and tested between 8–10 h post mortem, which is a time interval also used in other porcine ocular tissue studies [36–38]. To investigate the possible swelling of the corneal tissue after death, a baseline central corneal thickness (CCT) measurement was taken at the abattoir facility using a cornea-gage ultrasound pachymeter (Sonogage, Cleveland, Ohio), which employs a 50Mhz measurement frequency and assumes a speed of sound in corneal tissue of 1636 m/s. Five thickness measurements were taken of the central cornea for each of the globes and their average was calculated. They were repeated by touching the probe (held perpendicular to the cornea) to the central cornea until a measurement was recorded by the instrument and repeated in the same location four more times. Given the manual nature of the measurements, it was possible that there might be human error which is why there was a higher frequency of measurements and the average taken. Each cornea remained in air (out of the saline solution) for the duration of the OCE imaging sequence, which was approximately 3 min. The experiment was conducted in the same room, where the temperature and humidity were controlled. The average (SD) temperature and humidity in the measurement room during testing of the tissue were 23 (1) ° Celsius and 53 (5) % respectively.

3. Results

This study focused on assessing the use of static compression OCE to measure the Young's modulus of the *ex-vivo* porcine cornea. Table 1 provides a summary of the structural metrics for each of the individual samples. To assess the structural change in tissue, three metrics are reported; the average central corneal thickness (CCT) recorded at the abattoir facility using the ultrasound probe, the average corneal thickness (CT) of the pre-load image captured with the OCT, and the change in thickness (ΔT) between these two metrics (with a positive ΔT value indicating a swelling of the cornea). The CT measurements were corrected for corneal refractive index before comparison to ensure an accurate thickness was recorded. Overall, a tissue thickening (swelling) can be observed between the measure taken at the abattoir and the first OCE recording, with an average increase in thickness of 0.19 mm, which corresponds to about 20 % of the initial average thickness. This indicates that the corneas swelled during transport and dissection. Care should be

Table 1
Corneal metrics including CCT, CT, CT2 and change in thickness (ΔT) between CCT and CT.

Cornea	CCT (mm)	CT (mm)	CT2 (mm)	ΔT (mm)
1	1.125	1.328	1.151	0.203
2	0.976	1.363	1.153	0.387
3	0.811	1.316	1.073	0.505
4	0.945	1.169	1.073	0.224
5	1.093	1.164	1.136	0.071
6	1.089	1.041	0.986	−0.048
7	n.r.	1.149	1.071	–
8	0.965	1.014	0.908	0.049
9	0.874	1.146	1.038	0.272
10	1.044	1.100	0.987	0.056
Average	0.991	1.179	1.058	0.191

exercised while assessing this change, since the two instruments are based on different principles (a study by Cheong et al. [39] reported a difference of only a few μm between a Spectralis OCT and an ultrasound pachymetry instrument) and the CT may not represent the true thickness as the tissue is under a pre-load. Therefore, the results may potentially be under-reporting the degree of swelling. Despite these limitations, under the current tissue preparation protocol the sample experienced some swelling prior to the imaging process, which may impact the measurements.

CCT is the average of the 5 measurements taken at the abattoir facility using the Ultrasound probe. CT is the average initial pre-load thickness measured by the OCT approximately 8 h after harvesting. CT2 is the thickness of the cornea under compression during the first trial. ΔT is the change in thickness between CCT and CT. 'n.r.' indicates a not recorded value due to the instrument not recognising the thickness. '–' indicates not able to be determined.

To understand any potential structural changes in the tissue between OCE trials, the average first and last thickness values captured with the OCT instrument whilst under full compression were plotted (Fig. 3). For this figure, the compression thicknesses (CT2) were reported as opposed to the pre-load values, this was selected since the compressed cornea was subjected to the same load and it should provide a more standardised assessment.

As seen in Fig. 3, most of the corneas present a similar gradient of change, which indicates that the thickness needed to achieve the same level of force decreased between the initial and the final (third) OCE trial. This decrease in thickness can be observed in all but one of the corneas (cornea 8). Similarly, when investigating the Young's modulus between the initial and final trials, a positive trend is observed for most of the corneas, where the final Young's modulus value is larger than the initial. An analysis of covariance was conducted to examine the relationship between the change in Young's modulus and the change in corneal thickness, using the methods of [40]. This analysis showed a moderate but significant association between the change in the two parameters ($p = 0.015$, $R^2 = 0.274$), indicating that a reduction in corneal thickness is associated with a significant increase in Young's Modulus ($\beta = -0.0008$). It is likely that fluid within the corneal tissue, is being pushed out of the cornea during the static compression, and that this causes the observed thickness change. As water is an incompressible fluid [41], it gets pushed out of the corneal tissue during loading, reducing the thickness over the multiple trials. As the thickness decreased for the majority of corneas by a similar magnitude it suggests

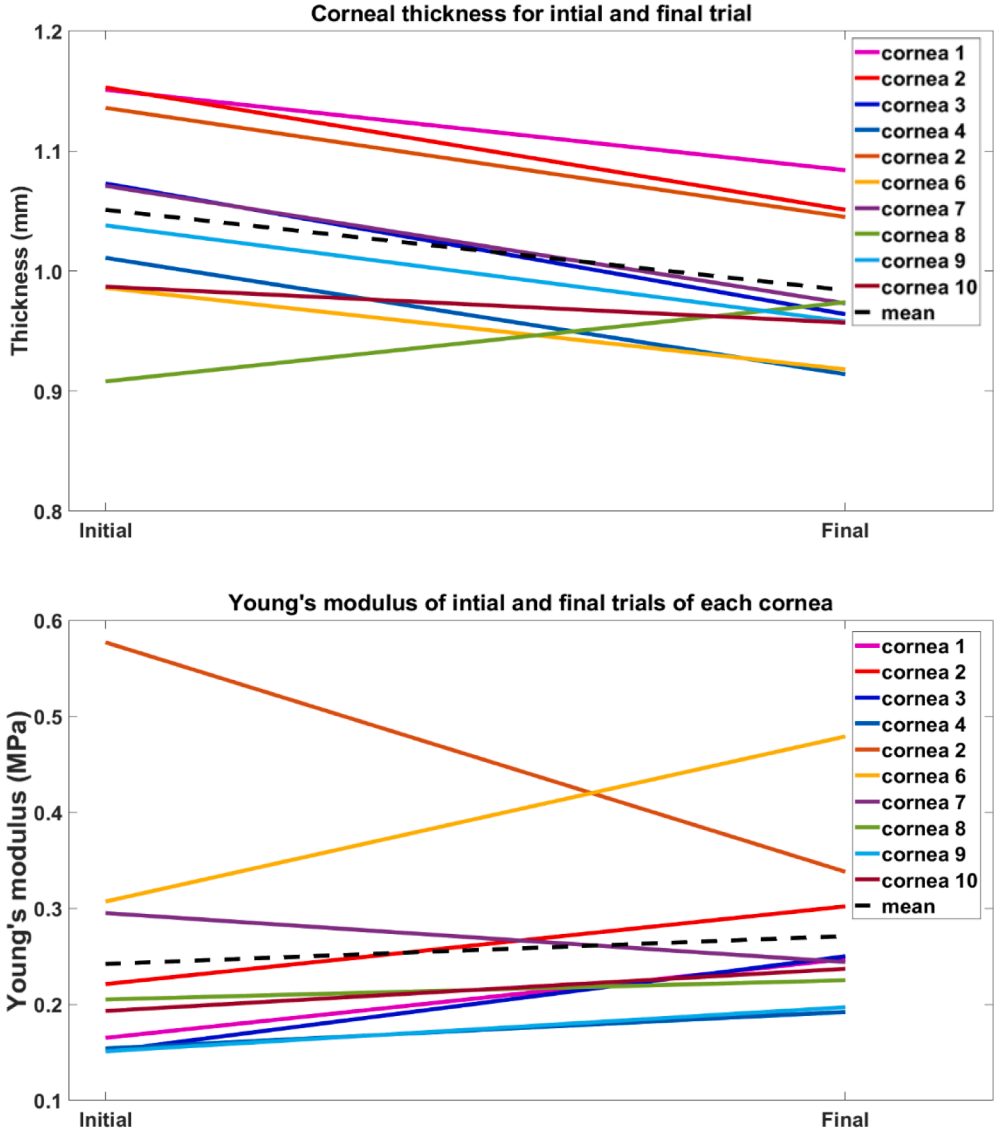

Fig. 3. Corneal thickness during compression for the initial and final trials (top). Young's modulus for the initial and final trials (bottom).

that approximately the same ratio of water was being pushed out. All corneas (apart from 8 & 10) experienced a reduction of thickness (as percentage difference) between 2.73 to 8.53 % when compared to their initial pre-load thickness (CT). The mean (SD) of the reduction in thickness was 6.87 (1.78) %.

After comparing the cornea means against the population mean using a one-sample *t*-test, it was determined that nine out of ten of the corneas were not statistically significantly different ($p > 0.05$) when comparing the Young's modulus values (only cornea # 4 was statistically different). While assessing the change in the Young's modulus between the repeated OCE trials on each cornea, on average a Young's modulus change of 0.029 MPa was observed between the trial. This reflects a positive increase between trial 1 and 3 which accounts for 10.88 % of the average Young's modulus. This large variance in the Young's modulus is likely linked to the previously mentioned tissue thickness changes between trials. The within population and within eye standard deviation were comparable to each other with only a difference of 0.027 MPa. The coefficient of repeatability showed that there were some variations between the different corneas ranging from 0.057 to 0.501 MPa. This variation is most likely due to the differences in the corneal properties between different porcine specimens. The overall COR was within the range of that shown by this method previously and shows a good trend that continues to support the validity of this method with viscoelastic tissue (Table 2).

Fig. 4 shows the relationship between the Young's modulus and the strain of each individual trial. The result suggests that there must be a change in the perceived mechanical properties between each trial. However, the graph shows that as the strain decreases the Young's modulus increases. Since the applied compressive force is kept constant between each trial based upon the force sensor recording, the result suggests that there must be a change in the measured mechanical properties between each trial. This could be related to the stress distribution given the change in thickness or it may be linked to the fluid content change between the trials, that is altering the tissue's measured mechanical properties We hypothesise that the compression is moving fluid out of the cornea and as more fluid is removed, more corneal cells are being compressed leading to a lower strain and a higher Young's modulus. A similar outcome has been reported by another study [27], in which a compressive test was applied to investigate the thickness of porcine corneas against the Young's modulus. A comparable effect was observed in this study, as the thicker the material increased due to swelling, the tissue exhibited a lower modulus. Whilst this phenomenon was noted during this study due the corneal buttons being dissected, this is unlikely to impact future *in-vivo* testing, since compression of the *in-vivo* cornea should not impact its water content.

4. Discussion

Direct comparisons between the Young's modulus values obtained from this compression OCE method to those from previous studies are difficult given the large differences in the experimental protocols, sample preparation and instrumentation used across the previous studies. However, to put our findings into perspective, a range of Young's modulus values reported in other studies were compared with the current results, while highlighting the key difference between studies (Table 3).

A study by Hatami-Marbini et al. [27] showed that the Young's modulus of excised porcine corneas ranged between 0.1 MPa and 0.5 MPa using a compressive shear test. These results exhibited varying thicknesses due to corneal swelling. Elsheikh et al. [37] used tensile testing to investigate the Young's modulus of porcine corneal strips. For a stress of 0.01 MPa, which was on average 5 % of the stress in this study, the Young's modulus of the tissue was 0.343 MPa. The corneal strips were immersed in fluid and the average thickness of the strips measured before dissection was 0.955 mm. Zhou et al. [45] used ultrasound imaging and vibrational loading to measure the modulus of elasticity in porcine globes that were maintained at a constant IOP using an infusion pump. The study showed that the Young's modulus of the cornea was 0.265 MPa. Whilst the studies presented each used different methods and applied different types and magnitudes of loading, the range of reported Young's modulus values (0.1 to 0.5 MPa) are in the same range as those determined from the current study (0.17 to 0.47 MPa).

As previously discussed, there are several limitations regarding the method and the materials tested that should be considered, especially with regards to the biological tissue. As the stress is assumed to be the same throughout the tissue, the reported values will not accurately represent the true stress across the tissue cross-section or its multiple layers. Additionally, due to the arrangement of the stromal fibrils, the cornea exhibits anisotropic properties, meaning that corneas will have a different Young's modulus in the longitudinal and axial directions. As such, only a compressive load can be used as a comparison. Currently, these is no way (apart from *ex-vivo* destructive testing) that allows for tensile testing *in-vivo* [46]. Finally, as the cornea exhibits non-linear viscoelastic properties, it is assumed that their properties do not impact the region of strain that is being measured.

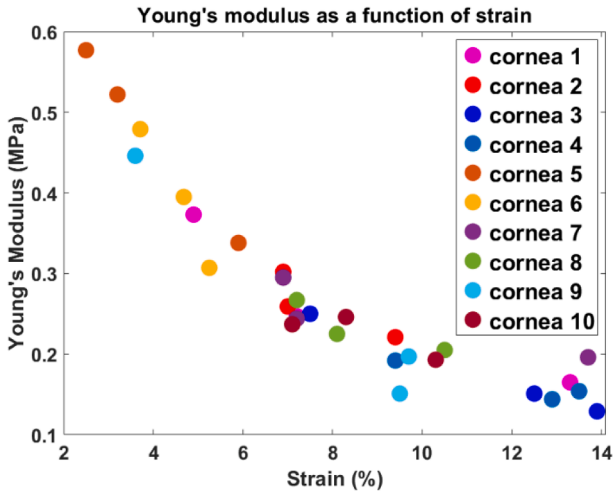

Fig. 4. Corneal Young's modulus as a function of strain for all 30 trials.

Table 2
Average Young's modulus of each cornea tested with population average (SD) extracted from the 3 trials for each cornea, within corneal standard deviation (S_w) and coefficient of repeatability (COR).

Cornea	Young's modulus (SD) (MPa)	S_w (MPa)	COR (MPa)
1	0.262 (0.105)	0.085	0.237
2	0.261 (0.041)	0.033	0.092
3	0.177 (0.065)	0.053	0.146
4	0.163 (0.026)	0.021	0.057
5	0.479 (0.125)	0.102	0.283
6	0.393 (0.086)	0.181	0.501
7	0.245 (0.049)	0.040	0.112
8	0.233 (0.032)	0.026	0.072
9	0.265 (0.158)	0.129	0.360
10	0.225 (0.029)	0.023	0.064
Average	0.271 (0.091)	0.118	0.329

Table 3
Young's modulus of porcine corneas from various studies.

Mode of testing	Young's modulus (MPa)
Compressive shear [27]	0.1 – 0.5
Tensile [37]	0.343 (0.064)
Vibrational [42]	0.265
Air puff with finite element analysis [43]	0.687
Inflation [44]	1.11
Current study	0.271 (0.091)

While the recorded tissue thickness changes (swelling prior to OCT data collection ~ 20 % and thinning during the OCT trials ~ 14 %) are likely to affect the mechanical properties of the tissue, the calculated values are comparable to those reported in the literature. Future experiments utilising measures on an intact globe are likely to reduce some of these unwanted structural changes. Another limitation is the inability to compare the metric with other elastography techniques on the same sample. Given the invasive and destructive nature of most elastography methods, this was not viable for this experiment.

As the current results showed that the average Young's modulus was within the values reported by other studies (for both compression and tension), the method was deemed viable to estimate the Young's modulus of corneal buttons of porcine tissue. Changes in tissue thickness and structural integrity (e.g., fluid content) are likely to influence the mechanical behaviour of the excised sample. Given the simple nature of this method, validation of animal tissue was an important step in showing that this approach can accurately measure the mechanical properties of a biological material that is viscoelastic. The results validated the assumption that ex-vivo porcine cornea is homogenous in nature and there is little variation within the microstructure. The contact OCE method described in this work could have significant advantages over some non-contact methods. The ability to control the loading methods manually can result in reduced artifacts and noise. The contact nature of the method also allows for individual calibration and standardisation due to the force application and would allow for a more standardised parameter to be measured across different studies but may be more invasive than non-contact methods. Future studies could investigate the use of optical palpation [22]. This would eliminate the need for an electronic force sensor to measure the stress of the loading to advance the method towards possible *in-vivo* applications, since an electronic force sensor cannot be easily implemented into an *in-vivo* method.

5. Disclosures

The authors have no relevant financial interests in this article and no potential conflicts of interest to disclose. The authors would like to acknowledge that this presented manuscript is a modified version of a chapter in the lead authors PhD thesis [31].

CRediT authorship contribution statement

Zachery Quince: Writing – review & editing, Writing – original draft, Validation, Software, Resources, Project administration, Methodology, Investigation, Formal analysis, Conceptualization. **David Alonso-Caneiro:** Writing – review & editing, Supervision, Software, Project administration, Methodology, Formal analysis, Conceptualization. **Scott A. Read:** Writing – review & editing, Supervision, Project administration, Formal analysis, Conceptualization. **Damien G. Harkin:** Writing – review & editing, Resources, Project administration, Conceptualization. **Michael J. Collins:** Writing – review & editing, Supervision, Resources, Investigation, Conceptualization.

Declaration of competing interest

The authors declare that they have no known competing financial interests or personal relationships that could have appeared to influence the work reported in this paper.

References

[1] Elsheikh A, Geraghty B, Rama P, Campanelli M, Meek KM. Characterization of age-related variation in corneal biomechanical properties. J R Soc Interface 2010;7(51):1475–85.

[2] Piñero DP, Alcón N. Corneal biomechanics: a review. Clinical Experimental Optometry 2015;98(2):107–16.

[3] Kirby MA, et al. Optical coherence elastography in ophthalmology. J Biomed Opt 2017;22(12):121720.

[4] Kennedy BF, Kennedy KM, Sampson DD. A review of optical coherence elastography: fundamentals, techniques and prospects. IEEE J Sel Top Quantum Electron 2014;20(2):272–88.

[5] Kling S, Hafezi F. Corneal biomechanics–a review. Ophthalmic Physiological Optics 2017;37(3):240–52.

[6] Ahearne M, Yang Y, Then KY, Liu K-K. An indentation technique to characterize the mechanical and viscoelastic properties of human and porcine corneas. Ann Biomed Eng 2007;35(9):1608–16.

[7] Hatami-Marbini H. Viscoelastic shear properties of the corneal stroma. J Biomech 2014;47(3):723–8.

[8] Kling S, Torres-Netto EA, Spiru B, Sekundo W, Hafezi F. Quasi-Static optical coherence elastography to characterize human corneal biomechanical properties. Investigative Ophthalmology Visual Sci 2020;61(6):29.

[9] Lan G, Aglyamov SR, Larin KV, Twa MD. In vivo human corneal shear-wave optical coherence elastography. Optom Vis Sci 2021;98(1):58–63.

[10] Wang S, Larin KV. Noncontact depth-resolved micro-scale optical coherence elastography of the cornea. Biomed Opt Express 2014;5(11):3807–21.

[11] Twa MD, et al. Spatial characterization of corneal biomechanical properties with optical coherence elastography after UV cross-linking. Biomed Opt Express 2014;5(5):1419–27.

[12] Wang S, Larin KV. Shear wave imaging optical coherence tomography (SWI-OCT) for ocular tissue biomechanics. Opt Lett 2014;39(1):41–4.

[13] Dorronsoro C, Pascual D, Pérez-Merino P, Kling S, Marcos S. Dynamic OCT measurement of corneal deformation by an air puff in normal and cross-linked corneas. Biomed Opt Express 2012;3(3):473–87.

[14] Zvietcovich F, et al. Confocal air-coupled ultrasonic optical coherence elastography probe for quantitative biomechanics. Opt Lett 2020;45(23):6567–70.

[15] McAuley R, et al. Co-axial acoustic-based optical coherence vibrometry probe for the quantification of resonance frequency modes in ocular tissue. Sci Rep 2022;12(1):18834.

[16] Kling S. In-vivo measurement of ocular deformation in response to ambient pressure modulation. Front Bioeng Biotechnol 2021;9:759588.

[17] Ford MR, Dupps WJ, Rollins AM, Roy AS, Hu Z. Method for optical coherence elastography of the cornea. J Biomed Opt 2011;16(1):016005.

[18] Ramier A, Tavakol B, Yun S-H. Measuring mechanical wave speed, dispersion, and viscoelastic modulus of the cornea using optical coherence elastography. Opt Express 2019;27(12):16635–49.

[19] Ramier A, et al. In vivo measurement of shear modulus of the human cornea using optical coherence elastography. Sci Rep 2020;10(1):17366.

[20] De Stefano VS, Ford MR, Seven I, Dupps WJ. Depth-dependent corneal biomechanical properties in normal and keratoconic subjects by optical coherence elastography. Translational Vision Sci Technol 2020;9(7):4.

[21] Quince Z, Alonso-Caneiro D, Read SA, Collins MJ. Static compression optical coherence elastography to measure the mechanical properties of soft contact lenses. Biomed Opt Express 2021;12(4):1821–33.

[22] Quince Z, Alonso-Caneiro D, Read SA, Collins MJ. Quantitative compressive optical coherence elastography using structural OCT imaging and optical palpation to measure soft contact lens mechanical properties. Biomed Opt Express 2021;12(12):7315–26.

[23] Jin Z, Zhou Y, Shen M, Wang Y, Lu F, Zhu D. Assessment of corneal viscoelasticity using elastic wave optical coherence elastography. J Biophotonics 2020;13(1):e201960074.

[24] Meng F, Zhang X, Wang J, Li C, Chen J, Sun C. 3D strain and elasticity measurement of layered biomaterials by optical coherence elastography based on digital volume correlation and virtual fields method. Appl Sci 2019;9(7):1349.

[25] Singh M, et al. Noncontact elastic wave imaging optical coherence elastography for evaluating changes in corneal elasticity due to crosslinking. IEEE J Sel Top Quantum Electron 2016;22(3):266–76.

[26] Ko H-J, Tan W, Stack R, Boppart SA. Optical coherence elastography of engineered and developing tissue. Tissue Eng 2006;12(1):63–73.

[27] Hatami-Marbini H, Etebu E. Hydration dependent biomechanical properties of the corneal stroma. Exp Eye Res 2013;116:47–54.

[28] Sridhar MS. Anatomy of cornea and ocular surface. Indian J Ophthalmol 2018;66(2):190.

[29] Alonso-Caneiro D, Read SA, Collins MJ. Automatic segmentation of choroidal thickness in optical coherence tomography. Biomed Opt Express 2013;4(12):2795–812.

[30] Chiu SJ, Li XT, Nicholas P, Toth CA, Izatt JA, Farsiu S. Automatic segmentation of seven retinal layers in SDOCT images congruent with expert manual segmentation. Opt Express 2010;18(18):19413–28.

[31] Quince Z. Optical coherence elastography for the measurement of anterior segment biomechanical properties. Queensland University of Technol 2022.

[32] Wollensak G, Spoerl E, Seiler T. Stress-strain measurements of human and porcine corneas after riboflavin–ultraviolet-A-induced cross-linking. J Cataract Refractive Surgery 2003;29(9):1780–5.

[33] Yazdi AA, et al. Characterization of non-linear mechanical behavior of the cornea. Sci Rep 2020;10(1):1–10.

[34] Zeng Y, Yang J, Huang K, Lee Z, Lee X. A comparison of biomechanical properties between human and porcine cornea. J Biomech 2001;34(4):533–7.

[35] Kling S, Marcos S. Effect of hydration state and storage media on corneal biomechanical response from in vitro inflation tests. J Refract Surg 2013;29(7):490–7.

[36] Elsheikh A, Alhasso D, Rama P. Biomechanical properties of human and porcine corneas. Exp Eye Res 2008;86(5):783–90.

[37] Elsheikh A, Alhasso D. Mechanical anisotropy of porcine cornea and correlation with stromal microstructure. Exp Eye Res 2009;88(6):1084–91.
[38] Hatami-Marbini H, Etebu E, Rahimi A. Swelling pressure and hydration behavior of porcine corneal stroma. Curr Eye Res 2013;38(11):1124–32.
[39] Cheong YJ, Lee BR, Han KE, Jun RM. Corneal thickness measurements using 2 kinds of spectral domain optical coherence tomography, pentacam, ultrasound pachymetry. J Korean Ophthalmological Society 2016;57(10):1527–34.
[40] Bland JM, Altman DG. Calculating correlation coefficients with repeated observations: Part 2—correlation between subjects. BMJ 1995;310(6980):633.
[41] Lind S, Stansby P, Rogers B, Lloyd P. Numerical predictions of water–air wave slam using incompressible–compressible smoothed particle hydrodynamics. Appl Ocean Res 2015;49:57–71.
[42] Zhou B, Sit AJ, Zhang XJU. Noninvasive measurement of wave speed of porcine cornea in ex vivo porcine eyes for various intraocular pressures. Ultrasonics 2017; 81:86–92.
[43] Bronte-Ciriza D, et al. Estimation of scleral mechanical properties from air-puff optical coherence tomography. Biomed Opt Express 2021;12(10):6341–59.
[44] Kling S, Ginis H, Marcos S. Corneal biomechanical properties from two-dimensional corneal flap extensiometry: application to UV-riboflavin cross-linking. Invest Ophthalmol Vis Sci 2012;53(8):5010–5.
[45] Campigotto A, Leahy S, Zhao G, Campbell RJ, Lai Y. Non-invasive Intraocular pressure monitoring with contact lens. Br J Ophthalmol 2019 (pp. bjophthalmol-2018-313714).
[46] Webb JN, Zhang H, Roy AS, Randleman JB, Scarcelli G. Technology, detecting mechanical anisotropy of the cornea using brillouin microscopy. Translational Vision Sci 2020;9(7):26.